IEEE Photonics Journal
An IEEE Photonics Society Publication

Open Access

Enhancement of the Dynamic Range in Slope-Assisted Coherent Brillouin Optical Time-Domain Analysis Sensors

Volume 9, Number 3, June 2017

Jon Mariñelarena
Javier Urricelqui
Alayn Loayssa, ***Member, IEEE***

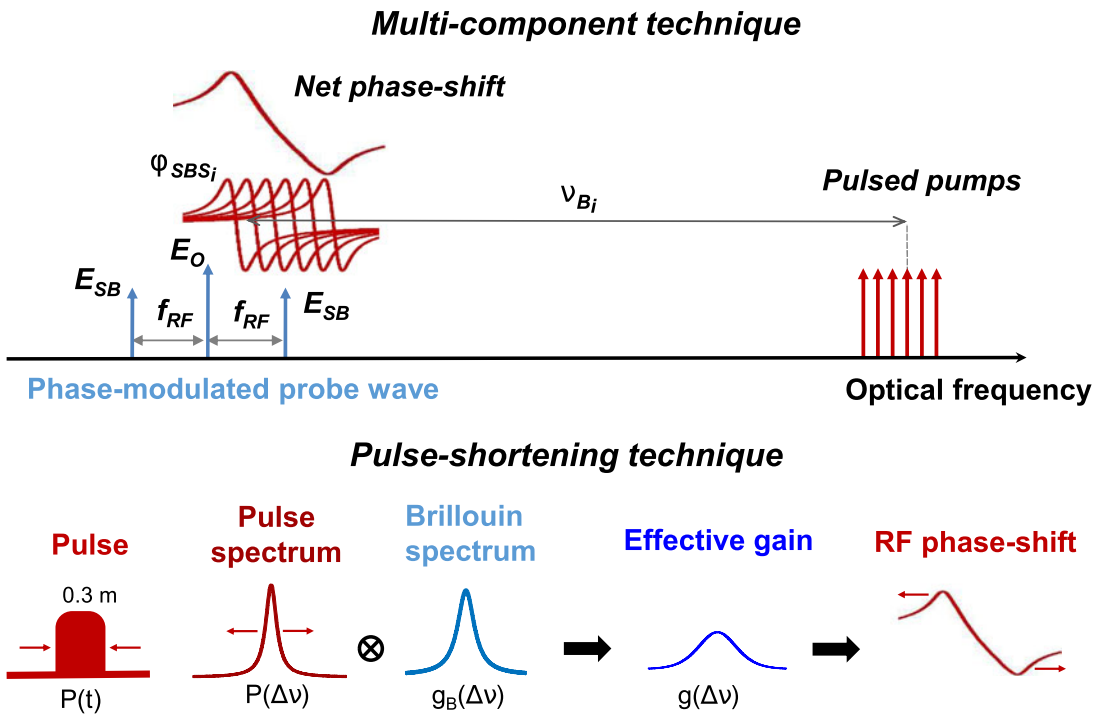

DOI: 10.1109/JPHOT.2017.2701203
1943-0655 © 2017 IEEE

IEEE photonics SOCIETY

IEEE

Enhancement of the Dynamic Range in Slope-Assisted Coherent Brillouin Optical Time-Domain Analysis Sensors

Jon Mariñelarena, Javier Urricelqui, and Alayn Loayssa, *Member, IEEE*

Department of Electrical and Electronic Engineering, Universidad Pública de Navarra, Pamplona 31006, Spain

DOI:10.1109/JPHOT.2017.2701203

Manuscript received March 17, 2017; revised April 17, 2017; accepted April 29, 2017. Date of publication May 4, 2017; date of current version May 19, 2017. This work was supported in part by the Universidad Pública de Navarra, in part by the Feder funds, and in part by the Spanish Ministerio de Economía y Competitividad through Project TEC2013-47264-C2-2-R and Project TEC2016-76021-C2-1-R. Corresponding author: Jon Mariñelarena (e-mail: jon.marinelarena@unavarra.es).

Abstract: We present two techniques that provide an extension of the dynamic range of coherent Brillouin optical time-domain analysis (BOTDA) sensors for dynamic measurements. These types of BOTDA sensors rely on self-heterodyne detection of a phase-modulated probe wave, and the dynamic range for fast measurements is limited to the linear region of the radio-frequency (RF) phase-shift spectrum measured. The first method for range extension that we introduce is based on launching pump pulses containing multiple frequency components. This makes the Brillouin spectra generated by each component overlap, providing a wider linear region of the detected RF phase-shift spectrum and allowing measurement of larger Brillouin frequency shift variations. The second method relies on shortening the length of the pump pulses, which leads to the broadening of the detected RF spectra. The theoretical fundamentals of both range enhancing techniques are presented. Moreover, we experimentally demonstrate that they provide a threefold to fourfold enhancement in the dynamic range. Finally, the factors limiting their performance are determined: For the multi-frequency pump pulse technique, it is the worsening of Kerr nonlinear effects due to the simultaneous propagation of multiple spectral components in the fiber, and for the pulse-shortening method, it is the signal-to-noise ratio (SNR) penalty linked to the reduction of the magnitude of the Brillouin interaction.

Index Terms: Dynamic range, Brillouin optical time-domain analysis (BODTA), dynamic coherent BOTDA sensor.

1. Introduction

Brillouin optical time-domain analysis (BOTDA) sensors have been established during the last years as a powerful technique for structural health monitoring that potentially could provide dynamic measurements of strain along structures such as wind-turbines, airplane wings, civil engineering structures, and others. Several methods have been recently presented to allow such fast dynamic measurements using the BOTDA principle [1]–[4]. Among them, the slope-assisted methods stand out as a simple solution to perform real-time measurements without increasing the complexity of the BOTDA setup [1], [4]. They are based on the frequency discriminator principle in which the probe

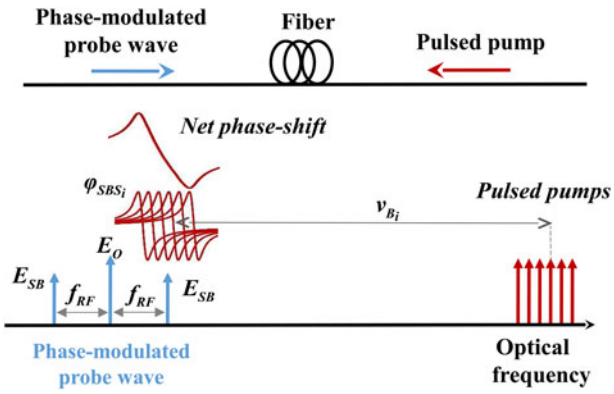

Fig. 1. Fundamentals of the multi-frequency components pump technique.

wave is set on the slope of the Brillouin gain spectrum (BGS) and the amplitude of the detected signal is interrogated so that variations of the Brillouin frequency shift (BFS) due to temperature or strain changes are translated to variations in the amplitude of the detected probe wave.

However, slope-assisted BOTDA sensors face several limitations. One of the most significant is the dependence of the BGS amplitude on the optical pump power. Hence, variations of the pump power level due to, for instance, changes in the attenuation of the fiber, may be wrongly interpreted as BFS variations caused by temperature or strain changes. This inconvenient has been partially mitigated with the double slope-assisted BOTDA technique [5], where both BGS slopes are measured, although the measurement time is also doubled.

Another fundamental limitation of the dynamic BOTDA sensors based on the slope-assisted technique is the reduced dynamic range that they provide. The dynamic range is defined by the linear region of the slope of the BGS, which depends on the BGS linewidth. For instance, for 10-ns pump pulse duration, the usable width of the BGS slope is typically around 50 MHz. This, assuming a 20 $\mu\varepsilon$/MHz strain coefficient, translates to a dynamic range of about 1000 $\mu\varepsilon$, which is insufficient for many structural health monitoring applications. This can be extended by switching the probe wave frequency in several steps within a given range, so that multiple BGS slopes can be interrogated [6], [7]. However, the measurement time also increases proportionally to the number of frequency steps. Another option is to deploy short pump pulses with the aim of broadening the BGS shape [8].

Recently, we have proposed a coherent BOTDA system based on slope-assisted method that uses a self-heterodyne detection of a phase-modulated probe wave [3]. This technique provides a very stable phase-shift response that shows very low dependence on the pump power [9]. Moreover, the linear region of the radio-frequency (RF) phase-shift spectra obtained from the detection of the RF signal approximately doubles the slope region of a conventional slope-assisted system.

In this work, we theoretically and experimentally study and compare two techniques to enlarge the dynamic range of the coherent BOTDA sensor for dynamic measurements. The first method is based on the generation of pump pulses containing multiple frequency components simultaneously, so as to synthesize a phase-shift slope that extends over a larger frequency region. The second technique used to improve the dynamic range involves the shortening of the pulse duration that permits to broaden the linear region of the RF phase-shift slope and, hence, provides a larger measurement region on coherent BOTDA systems.

2. Fundamentals of Dynamic Range Enhancement

2.1 Multi-Spectral Components Pump Pulses

Fig. 1 depicts the fundamentals of the first technique to extend the dynamic range that is proposed in this paper. It is based on the use of a pump pulse signal containing multiple frequency components

simultaneously, which is injected from one end of the fiber to interact with one of the sidebands of a phase-modulated probe wave injected from the other end. As it is schematically depicted in Fig. 1, the phase-shifts associated to the Brillouin spectra generated by the different pump components overlaps and give rise to an extended phase-shift spectrum. The frequency detuning between the multiple frequency components of the pump signal has to be adjusted depending on the particular linewidth of the Brillouin spectrum in order to optimize the extension of the phase-shift range.

The total Brillouin gain spectrum that results from the overlap of the n gain spectra generated by the interaction of the probe wave with a pump pulse having n spectral components is given by

$$H(\nu, z) = \exp\left(\sum_{i=1}^{n} G_i(\nu, z)\right) \tag{1}$$

where $H(\nu, z)$ is the Brillouin gain spectrum at position z, and $G_i(\nu, z)$ is the complex exponential Brillouin gain at position z induced by the i spectral component. In case the pump pulse durations employed are significantly longer than the phonon lifetime ($>$10 ns), the pulse spectral profile can be approximated by a Lorentzian shape and the expression becomes

$$H(\nu, z) = \exp\left(\sum_{i=1}^{n} g_{0_i} \frac{\Delta\nu_B}{\Delta\nu_B + 2j(\nu + \nu_{p_i} - \nu_B(z))}\right) \tag{2}$$

where g_{0_i} is the peak gain of the Brillouin interaction induced by the i spectral component, $\Delta\nu_B$ is the Brillouin frequency shift of the fiber under test at position z, and ν and ν_{pi} are the optical frequencies of the probe and the ith spectral component of the pump, respectively. In this work, we will be dealing with pulses with durations equal or shorter than the phonon lifetime ($\leq$10 ns), for which $G_i(\nu, z)$ strongly depends on the pump pulse spectrum and generally has not close-form expression. Hence, our approach will be to model $G_i(\nu, z)$ as the convolution of a Gaussian function, representing the pump pulse spectrum, and a Lorentzian function, which relates to the intrisic Brillouin gain spectra. The result is the so-called Faddeeva profile, which has been found to fit very well the experimental measurements of the complex Brillouin gain spectra generated by short pulses [9].

Fig. 2(a) depicts the calculated Brillouin amplitude spectra when pump pulses with several spectral components are counter-propagated to the probe wave. These spectra have been calculated modeling $G_i(\nu, z)$ as a Faddeeva profile with a linewidth of 90 MHz. Moreover, the different tones inside the pump pulse have been spaced by 55 MHz to ensure adequate overlapping of their BGS. As it is observed, the total Brillouin gain spectrum is broadened and flatten as the number of spectral components in the pulse increases. Moreover, the peak amplitude increase. However, note that the slope region of the spectra is not significantly broaden; hence this broadening would be useless for a conventional slope-assisted BOTDA sensor. Fig. 2(b) shows the Brillouin phase-shift spectra, where it can be seen that the slope region of the spectra has been broadened due to overlapping of the phase-shift spectra generated by each spectral component of the pump pulse. Therefore, these results hint that the multi-component pump method is going to be useful to extend the dynamic range of BOTDA sensors that rely on the Brillouin phase-shift, such as the coherent self-heterodyne BOTDA sensor.

In the coherent self-heterodyne BOTDA sensor, the phase-modulated probe wave, whose sideband has interacted with the multi-component pump, is detected in a photo-diode and the resultant RF signal is demodulated [3]. This signal is given by [9]

$$P(t)\Big|_{f_{RF}} = 2E_0E_{SB} \cdot \left[G_{SBS}\cos(2\pi f_{RF}t + \varphi_{SBS}) - \cos(2\pi f_{RF}t)\right] \tag{3}$$

where G_{SBS} and φ_{SBS} are the amplitude and phase-shift of the total Brillouin gain spectrum, f_{RF} is the phase modulation frequency of the probe wave, and E_0 and E_{SB} are the complex amplitudes of the carrier and sidebands. This expression can be used to calculate the resultant RF amplitude and RF phase-shift spectra as a function of the number of spectral components in the pump. Their

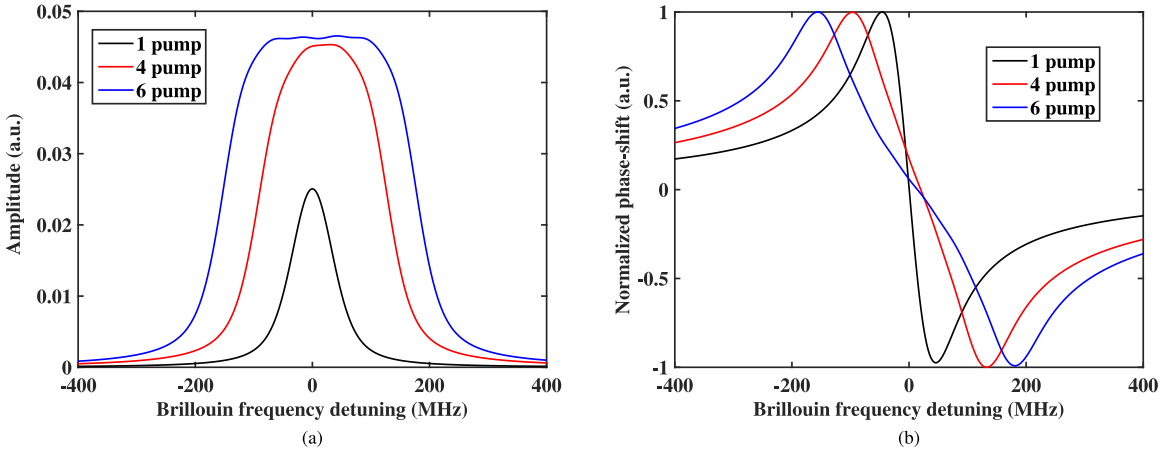

Fig. 2. Calculated results of the (a) Brillouin amplitude and (b) phase-shift spectra for different number of pump pulse frequencies. Separation between different tones of 55 MHz are used.

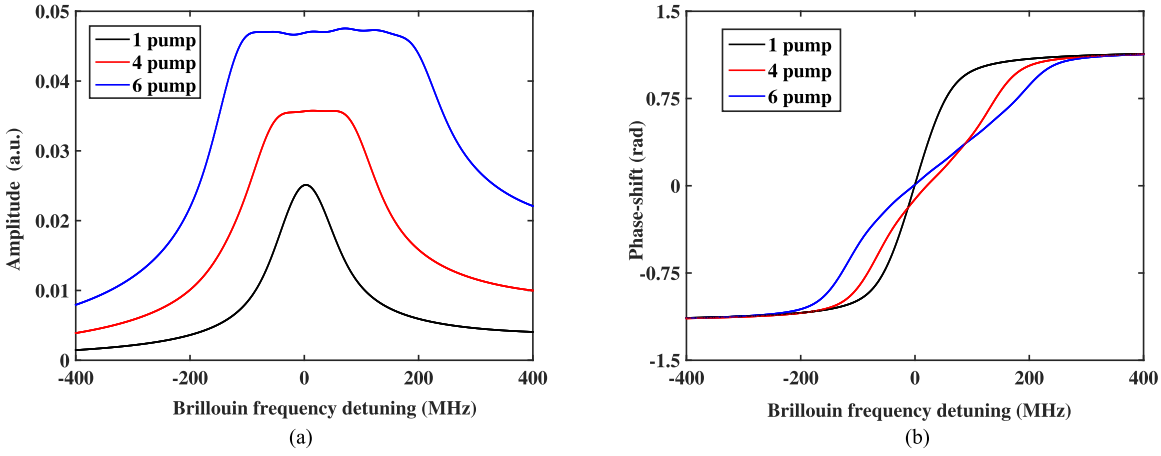

Fig. 3. Calculated results of the (a) RF amplitude and (b) RF phase-shift spectra for different number of pump pulse components.

RF amplitude and phase-shift expressions are

$$|P_{RF}| = E_0 E_{SB} \sqrt{[G_{SBS}(\cos(\varphi_{SBS}) - 1)]^2 + [G_{SBS} \sin(\varphi_{SBS})]^2} \tag{4}$$

$$\theta_{RF} = \arctan\left(\frac{G_{SBS} \cdot \sin(\varphi_{SBS})}{G_{SBS} \cdot \cos(\varphi_{SBS}) - 1}\right). \tag{5}$$

Fig. 3(a) and (b) shows the calculated spectral broadening using (4) and (5) when multiple pump pulse components are generated. Again, this calculation assumes a Faddeeva profile for $G_i(\nu, z)$. Notice that, similarly to the Brillouin phase-shift spectra, the RF phase-shift spectra shape becomes wider, providing a larger slope region. As it is observed, the slope is not purely linear, as it is the result of the self-heterodyne detection process of the phase-modulated probe wave. However, this is not an important issue because this slope can be calibrated and used for dynamic measurements as long as it has a monotonically increasing behavior. With regard to the amplitude spectrum, again a broadening and an increment of peak amplitude is observed. The latter is going to result in an enhancement of the detection signal-to-noise ratio (SNR). Observe that the detected RF amplitude spectrum shape shown in Fig. 3(a) slightly differs with the Brillouin gain spectrum shape shown in Fig. 2(a), which is due to the slight affectation of the modulated probe wave carrier with the Brillouin interaction that manifests after the heterodyne detection process of the RF signal [3].

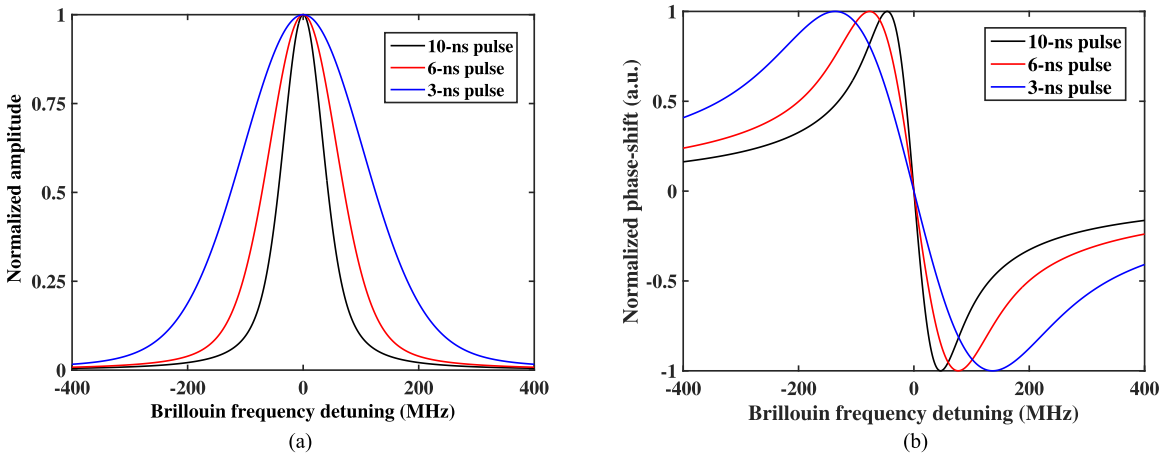

Fig. 4. (a) Brillouin gain and (b) phase-shift spectra broadening depending on the pulse duration.

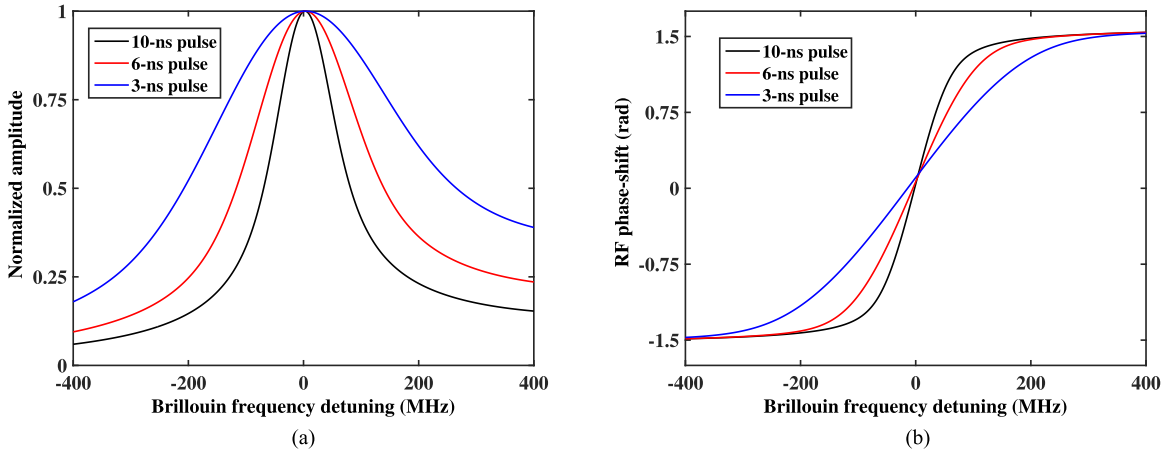

Fig. 5. (a) RF amplitude and (b) RF phase-shift spectra broadening depending on the pulse duration.

In principle, it could seem that the method just described could provided arbitrarily large dynamic range by simply adding sufficient spectral components to the pump pulse. However, in practice, as it will be shown in next section, nonlinear cross Kerr-effect interactions limit the number of spectral components that can be used [10]–[12].

2.2 Pulse Shortening Method

The second technique that we propose to extend the dynamic range of self-heterodyne BOTDA sensors is based on shortening the length of the pump pulses injected into the fiber. This technique takes advantage of the inverse dependence of the Brillouin gain linewidth on the pulse duration. For pump pulses shorter than 20 ns, the BGS linewidth $\Delta\nu_B$ is approximately given by $1/T$ [13].

Fig. 4(a) and (b) shows the broadening of the Brillouin gain and Brillouin phase-shift spectra when different pulse durations are generated. Since we evaluated this technique with short pump pulses (from 3-ns to 10-ns length), the BGS broadening has been calculated with (1) and assuming that the resultant gain spectra follow a Faddeeva profile, adjusting the pulse spectral width parameter of the Faddeeva function depending on the pulse duration employed. The broadening of the Brillouin amplitude and phase-shift spectra is translated to the detected RF signal. Fig. 5(a) and

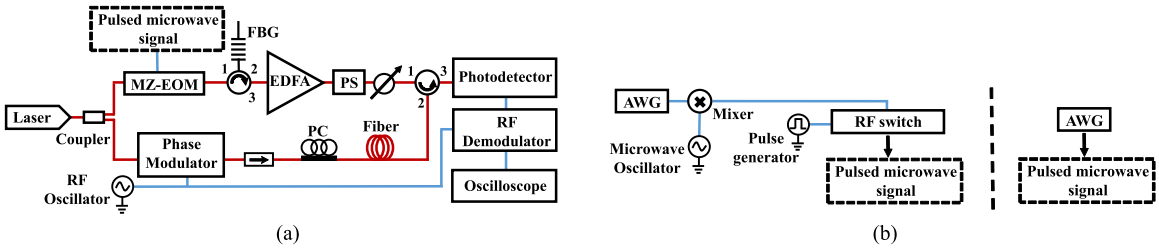

Fig. 6. (a) Experimental setup deployed for the extension of the dynamic range in coherent BOTDA sensors. (b) Microwave signal generation for the two presented techniques: multiple component pulse method (left-hand side) and shortening of pulses method (right-hand side).

(b) represents the broadening of the RF amplitude and RF phase-shift spectra as the pump pulses are shortened. As it is observed, the RF phase-shift spectrum becomes broader, providing a larger linear region of the phase-shift, what means that the dynamic range is enhanced.

Therefore, it is demonstrated that using the shortening of pulses technique is possible to enlarge the slope region of the RF phase-shift spectrum employed in the coherent self-heterodyne BOTDA sensors. However, the inherent broadening of the RF amplitude spectrum observed in Fig. 5(a) reduces the peak gain as well as the SNR, making the system more susceptible to noise.

3. Experimental Setup

Fig. 6(a) depicts the experimental setup deployed for this research, which is similar to the dynamic coherent BOTDA system with slight modifications setup [3], [9]. A distributed feedback laser (DFB) is used as an optical source. In the upper branch of the setup, optical pump pulses are generated using a Mach-Zehnder electro-optic modulator (MZ-EOM), which is biased at minimum transmission and driven by microwave pulses. As a result, a pulsed double-sideband suppressed-carrier (DSB-SC) pump signal is generated. The pulsed microwave signal is created in different ways depending on which technique is deployed. The left-hand side of Fig. 6(a) shows the experimental setup deployed for the generation of the microwave signal used in the multi-component pump technique. An arbitrary waveform generator (AWG) is used to generate the multiple RF tones at an intermediate frequency, which then are up-converted to the BFS band, using a mixer and a local microwave oscillator. Finally, these microwave signal is pulsed using an RF switch that is driven by a pulse generator and fed to the MZ-EOM. The pulsed microwave signal generation of the pulse-shortening method is simpler, as it can be seen in the right-hand side of Fig. 6(b). An arbitrary waveform generator (AWG) that directly forms very short microwave pulses has been deployed, replacing the mixer and the microwave switch from the first setup. Then this pulsed microwave signal drives the MZ-EOM.

Apart from the microwave signal generation, the rest of the setup is the same for both techniques. One of the two pu mp sidebands generated is filtered with a fiber Bragg grating (FBG), and the other is amplified by a high-power erbium doped fiber amplifier (EDFA). Then, an optical attenuator controls the pump power injected to the fiber, which can reach a peak value of 4 W. The polarization fluctuations are compensated using a polarization scrambler just before injecting the pump pulses into the fiber. In the lower branch, the phase-modulated probe wave is generated with an electro-optic phase modulator driven by an 1300 MHz RF signal. The power of the phase-modulated probe wave sidebands was set to -4 dBm, a safe enough power level to avoid non-local effects in this system [14]. Then, this signal is injected at the far end of the fiber under test (FUT). After interacting with the pump pulses in the FUT via stimulated Brillouin scattering (SBS), the resultant probe wave is directed to a receiver and the RF signal obtained is demodulated and captured in a digital oscilloscope employing 4000 averages.

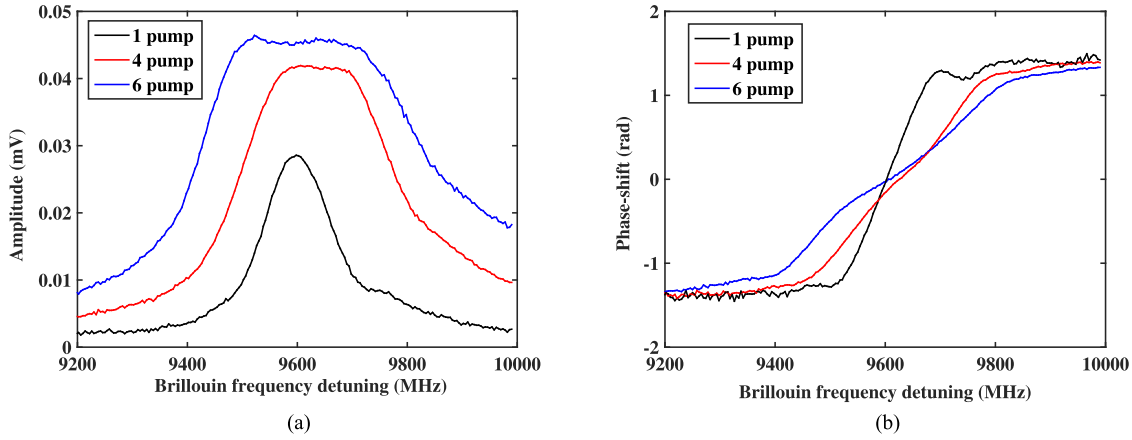

Fig. 7. Experimental results of the (a) RF amplitude (b) and phase-shift spectra for different number of pump pulse frequencies.

4. Experimental Results

In order to prove the validity of the multiple component pump pulses technique proposed to extend the dynamic range of the coherent self-heterodyne BOTDA sensor the following experimental measurements were performed. Fig. 7(a) and (b) shows the experimental RF amplitude and RF phase-shift spectra measured as a result of using 10-ns-length pulses with 1, 4 or 6 spectral components. The depicted spectra and the extension range results provided later were measured at 1-km fiber distance, which is long-enough to cover typical applications that require dynamic BOTDA sensors.

The pump peak power of each spectral component being pulsed was adjusted to 16 dBm and their frequency difference was set to 55 MHz, which approximately corresponds to half of the FWHM of the gain spectrum linewidth for 10-ns pulse duration. As it was expected, the more frequency components, the wider the RF amplitude and phase-shift spectra. Notice that the general shape of the RF phase-shift spectra measured experimentally and that shown in the calculations of Fig. 3 are very similar. The small differences stem from the fact that, as it was explained before, the complex BGS depends on the pulse spectrum, and it can only be approximately modeled as the convolution of a Gaussian and Lorentzian profiles. Notice also that the dynamic range is more than doubled when increasing the number of spectral components of the pump pulse from one to four, i.e. from 130 MHz to 300 MHz (from $\pm$1300 $\mu\varepsilon$ to $\pm$3000 $\mu\varepsilon$ assuming again a 20 $\mu\varepsilon$/MHz strain coefficient). Furthermore, with six spectral components the dynamic range is tripled, reaching around 400 MHz ($\pm$4000 $\mu\varepsilon$). Moreover, as it was mentioned before, the maximum peak amplitude of the detected RF amplitude spectrum increases when pulses with multiple frequencies are launched, improving the SNR in 1.7 dB when four spectral components are generated and in 2 dB when six are used.

However, there is an important limitation that affects the multi-component pulse technique. As multiple pump pulses are injected to the fiber, the maximum peak pump pulse power has to be reduced due to the modulation instability (MI) and four wave mixing (FWM) effects [10]–[12]. MI and FWM effects are directly dependent on the pump power injected to the fiber, inducing a depletion of the pump power along the fiber that reduces the interaction between the probe and pump waves. This depletion limits the performance of this system via the reduction of the SNR.

Fig. 8 depicts the normalized BOTDA traces of an 8-km spool fiber for different levels of pump peak power. All traces have been normalized to the peak power and the fiber attenuation has been compensated. This figure shows the pump power depletion along the fiber for a single spectral component pump pulse of 10-ns length due to MI. As it has been explained, there is a dependence of the pump depletion with the pump peak power injected to the fiber: the pump depletion becomes more severe as the pump peak power is increased [10]. Notice that in the traces of Fig. 8, there are

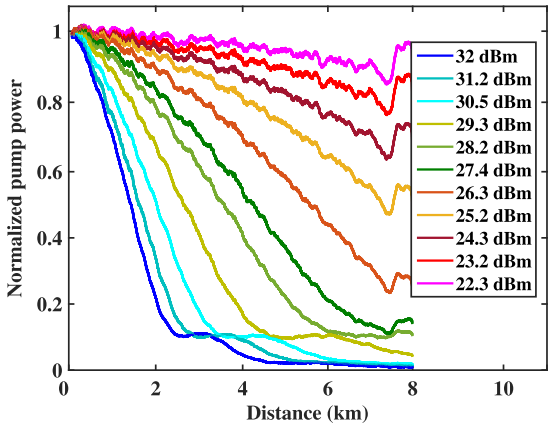

Fig. 8. Evolution of pump power along the fiber for a pulse with a single frequency component.

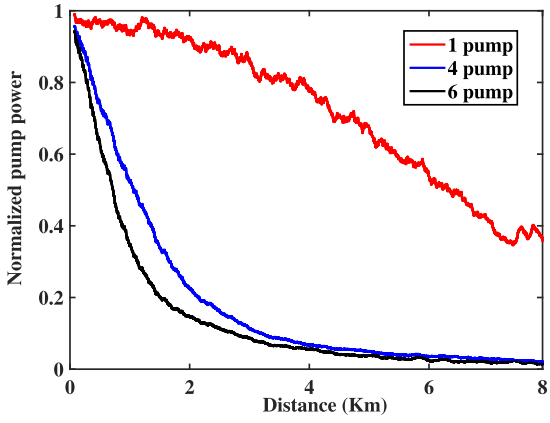

Fig. 9. Pump power depletion along the fiber for different number of pulse spectral components each with of 26 dBm peak power at the start of the fiber.

some variations in signal level at the few hundred meters of the end of the fiber that are not due to FWM or MI but to a BFS change due to the use of a different fiber type for this final section of the FUT.

Fig. 9 depicts how the pump depletion just analyzed is worsen as additional frequency components are added to the pump pulses. This penalty can be analyzed by considering the so-called critical pump power, which is defined as the maximum pump power that can be launched into a given length of fiber before the pump depletion at its end becomes larger than 10%. Fig. 10 depicts this parameter as a function of the fiber length and for different number of frequency components in the pump pulse. The resultant penalty in terms of power for the use of four and six-component pump pulses is around 9 dB and 11 dB, respectively. This SNR degradation is partially compensated with the increase of the RF amplitude spectrum level, due to the overlap of the multiple spectra generated by each pump component. This enhancement of the detected signal for both multi-component pump cases is 1.7 dB and 2 dB; hence, the net penalty of this method is 7.3 dB (4-component) and 9 dB (6-component), respectively.

Apart from the pump power limitations, another difficulty faced on the multiple component pump pulses method lies on its practical implementation. It was found that the generation of a closely-spaced set pure microwave pulses in a cost-effective manner was not trivial. Unavoidable spurious component generated in the microwave components, particularly the mixer, were found to contribute to the critical pump power penalty. Despite these drawbacks, the multi-component pump pulse

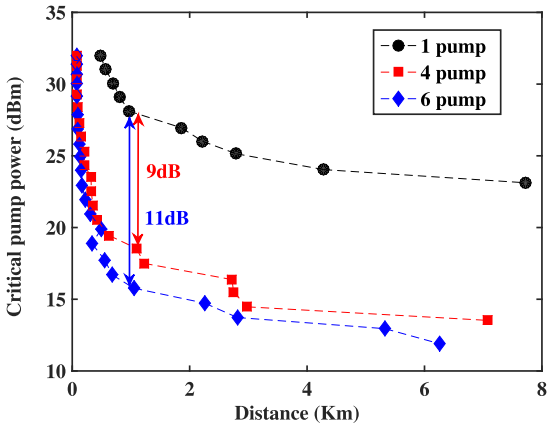

Fig. 10. Critical pump peak power depending on the distance for different number of pump pulse frequencies.

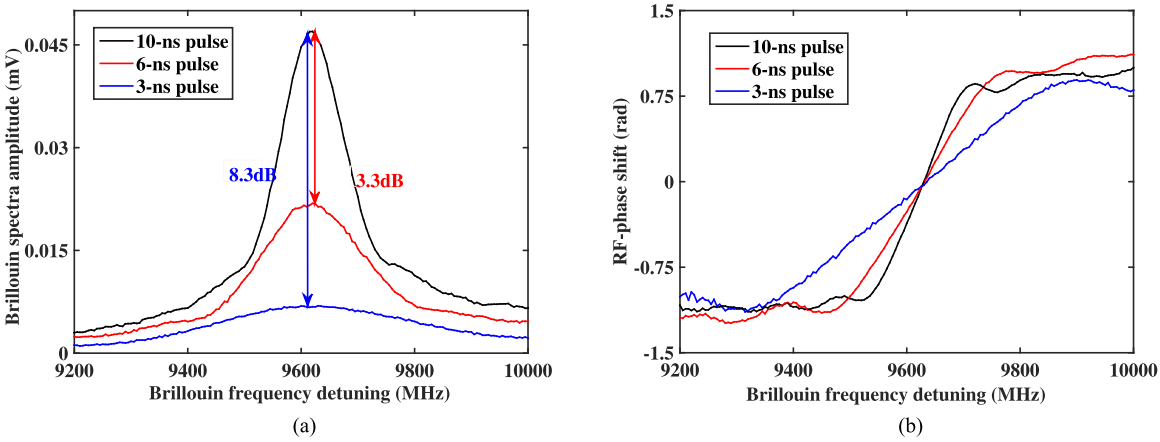

Fig. 11. (a) Experimental amplitude and (b) RF phase-shift spectra when short pulses are employed.

method provides a significant enhancement in the dynamic range with a power penalty that is tolerable for most short-distance dynamic strain measurement applications.

Regarding the second dynamic range enhancement tool, the pulse shortening method, we have experimentally measured the broadening of the RF phase-shift spectra with different pump pulse durations injected into the FUT. Fig. 11(b) and (b) depicts the resultant RF amplitude and phase-shift spectra measured at 1-km fiber distance when using 10-ns, 6-ns and 3-ns pulses. As it is observed, the RF phase-shift spectrum slopes are extended, obtaining more than an almost fourfold extension of the dynamic range when a 3-ns pulse is used compared to a 10-ns pulse: from 130 MHz ($\pm$1300 $\mu\varepsilon$) to 500 MHz ($\pm$5000 $\mu\varepsilon$).

The shortening of pulses provides an additional advantage, which is the potential enhancement of the spatial resolution. As the length of the pulses generated are shortened to 3-ns duration, the spatial resolution obtained in this system can be enhanced to 30 cm. Another important advantage with respect to the multiple component pump pulse technique is that there is no critical pump power penalty due to non-linear effects. This is because for the shortening of pulses method there is only one pump pulse component injected in the fiber. However, despite the lack of pump power penalty, the magnitude of the RF amplitude spectrum is reduced, and with it the noise in the RF phase-shift increased, due to the shortening of the interaction time between the probe wave and the pump pulse. The penalty for different pulse duration is shown in Fig. 11(a); for 3-ns pulses, the penalty compared to the use of 10-ns pulses rises to 8.3 dB. Since the SNR of the detected signal is

directly proportional to the root square of the number of averages [15], and thus, if the SNR penalty caused by using a shortened pulse is 8.3 dB, the number of averages should be increased about 45 times to maintain the system performance. As the measurement time is directly proportional to the number of averages, it also increases 45 times.

5. Conclusion

We have introduced two new techniques to extend the dynamic range of the coherent self-heterodyne BOTDA sensor. Experiments have demonstrated between a threefold and fourfold enhancement, mostly limited by the performance of the available components in the setup. In addition, both methods display a power penalty of the same order but with different origins. This makes both suitable for application in a multitude of dynamic strain and vibration measurements in the structural health monitoring field, where the SNR penalties involved are not very significant, considering that the lengths of fiber involved are usually small. Regarding the comparison of the two methods, their relative performance seems to slightly favor the pulse shortening over the multi-component pump method, particularly because of the spatial resolution enhancement that it provides. However, that performance greatly depends on the practical implementation of the electronic circuits involved in the generating the microwave pulses. Generating a low-cost multi-tone microwave signal seems relatively easier and cheaper than a very narrow microwave pulse with very small rise time. In fact, a possible middle ground could be found by combining both methods: Use a moderate number of spectral components in the pulse but shorten its duration so that each spectral component induces a broad spectrum that overlaps to provide a large overall dynamic range.

References

[1] R. Bernini, A. Minardo, and L. Zeni, "Dynamic strain measurement in optical fibers by stimulated Brillouin scattering," *Opt. Lett.*, vol. 34, no. 17, pp. 2613–2615, Sep. 2009.
[2] Y. Peled, A. Motil, and M. Tur, "Fast Brillouin optical time domain analysis for dynamic sensing," *Opt. Exp.*, vol. 20, no. 8, pp. 8584–8591, Apr. 2012.
[3] J. Urricelqui, A. Zornoza, M. Sagues, and A. Loayssa, "Dynamic BOTDA measurements based on Brillouin phase-shift and RF demodulation," *Opt. Exp.*, vol. 20, no. 24, pp. 26 942–9, Nov. 2012.
[4] Y. Peled, A. Motil, L. Yaron, and M. Tur, "Slope-assisted fast distributed sensing in optical fibers with arbitrary Brillouin profile," *Opt. Exp.*, vol. 19, no. 21, pp. 19 845–19 854, Sep. 2011.
[5] A. Motil, O. Danon, Y. Peled, and M. Tur, "Pump-power-independent double slope-assisted distributed and fast Brillouin fiber-optic sensor," *IEEE Photon. Technol. Lett.*, vol. 26, no. 8, pp. 797–800, Apr. 2014.
[6] D. Ba *et al.*, "Distributed measurement of dynamic strain based on multi-slope assisted fast BOTDA," *Opt. Exp.*, vol. 24, no. 9, pp. 9781–9793, May 2016.
[7] D. Zhou *et al.*, "Slope-assisted BOTDA based on vector SBS and frequency-agile technique for wide-strain-range dynamic measurements," *Opt. Exp.*, vol. 25, no. 3, pp. 1889–1902, Feb. 2017.
[8] Q. Cui, S. Pamukcu, W. Xiao, and M. Pervizpour, "Truly distributed fiber vibration sensor using pulse base BOTDA with wide dynamic range," *IEEE Photon. Technol. Lett.*, vol. 23, no. 24, pp. 1887–1889, Dec. 2011.
[9] J. Mariñelarena, J. Urricelqui, and A. Loayssa, "Gain dependence of the phase-shift spectra measured in coherent Brillouin optical time-domain analysis sensors," *J. Lightw. Technol.*, vol. 34, no. 17, pp. 3972–3980, Sep. 2016.
[10] M. Alem, M. Soto, and L. Thévenaz, "Analytical model and experimental verification of the critical power for modulation instability in optical fibers," *Opt. Exp.*, vol. 23, no. 23, pp. 29 514–29 532, Nov. 2015.
[11] J. Urricelqui, M. Alem, M. Sagues, L. Thévenaz, A. Loayssa, and M. Soto, "Mitigation of modulation instability in Brillouin distributed fiber sensors by using orthogonal polarization pulses," *Proc. SPIE*, vol. 9634, pp. 1–4, Oct. 2015.
[12] T. Horiguchi, K. Shimizu, T. Kurashima, M. Tateda, and Y. Koyamada, "Development of a distributed sensing technique using Brillouin scattering," *J. Lightw. Technol.*, vol. 13, no. 7, pp. 1296–1302, Jul. 1995.
[13] A. Motil, R. Hadar, I. Sovran, and M. Tur, "Gain dependence of the linewidth of Brillouin amplification in optical fibers," *Opt. Exp.*, vol. 22, no. 22, pp. 27 535–27 541, Nov. 2014.
[14] L. Thévenaz, S. F. Mafang, and J. Lin, "Effect of pulse depletion in a Brillouin optical time-domain analysis system," *Opt. Exp.*, vol. 21, no. 12, pp. 14 017–14 035, Jun. 2013.
[15] M. A. Soto and L. Thévenaz, "Modeling and evaluating the performance of Brillouin distributed optical fiber sensors," *Opt. Exp.*, vol. 21, no. 25, pp. 31 347–31 366, Dec. 2013.